

DESIGN AND DEVELOPMENT OF A MULTIPHASE INVERTER FOR AUTOMOTIVE APPLICATIONS

Rodrigo Parizotto¹, Evandro Claiton Goltz², Ederson dos Reis¹, Paulo Roberto Eckert¹

¹Universidade Federal do Rio Grande do Sul, Porto Alegre - RS, Brazil

²Universidade Federal de Santa Maria, Santa Maria - RS, Brazil

e-mail: roparizotto@gmail.com, evandro@inf.ufsm.br, edreis1510@gmail.com, paulo.eckert@ufrgs.br

Abstract – This work describes the development of a multiphase inverter that can operate as a platform for driving and testing electrical machines with up to 15 phases, in addition, it can operate with a fundamental frequency of up to 1 kHz and a switching frequency of 100 kHz. Therefore, a multiphase voltage source inverter (VSI) topology using SiC MOSFETs and approved components for automotive applications was designed and constructed. The developed platform is composed of independent power modules and a control module with technology that uses only a single microcontroller capable of generating all signals with pulse width modulation (PWM). To validate the inverter, experimental tests were carried out with a YASA (Yokeless and Segmented Armature) machine that can operate with 3, 5, or 15 phases and also with multi-star connections, one with three independent systems of five phases and another with five independent three-phase systems. Experimental results show that the inverter is capable of driving and testing multiphase machines with a wide variety of electrical connections using high fundamental and carrier frequencies. Therefore, the developed platform is an important tool that allows the testing of multiphase and multi-star electrical machines operating under the most diverse configurations and operating conditions.

Keywords – Automotive inverter, Multiphase inverter, Multi-star inverter, SiC MOSFET, YASA motor.

I. INTRODUCTION

Research in the area of electric vehicles has been promoting significant advances in the technology of batteries, electric machines and inverters, which are considered challenges for industrial competitiveness in the transition to clean energy. However, there are still significant technological challenges in the electric mobility sector, development of high power densities motors for direct drive systems, devices with high reliability, redundancy, high operating frequencies, fault tolerance, among others [1], [2].

Some aspects related to the mentioned challenges are overcome with the use of multiphase electrical machines that can operate under failure in one or more phases [3]. Concerning three-phase electrical machines, multiphase machines present a reduction in torque oscillation, noise, and phase currents (decreasing the stress on the inverter power

switches). Additionally, the power density of the electrical machine is increased [3], [4], [5].

Other relevant aspects, according to [6], are volume restrictions, weight reduction of electric machines, improvement in vehicle efficiency, and autonomy. An alternative to improve these last aspects is the emerging trend of several manufacturers to increase the mechanical speed of electrical machines (especially the permanent magnet synchronous ones) coupled with speed reduction mechanisms.

In [6], several commercial models, prototypes, and concepts of high-speed electrical machines (HSEM) are presented for application in electric vehicles (EVs) and hybrid electric vehicles (HEVs). Angular speed ranges from 10.000 rpm to 16.000 rpm are mentioned [6].

On AC machines, operation at high speeds requires a high fundamental operating frequency and a higher switching frequency. In this context, the new inverter topologies aimed at the application of control and drive of electrical machines in EVs and HEVs point to the use of components using materials technology with wide bandgap semiconductors technology, such as SiC MOSFET. These static power switches offer greater efficiency, higher power density, and can operate with higher switching frequency and in harsh environments. Therefore, they can provide a reduction in overall system costs and gains in quality and reliability, making it an attractive alternative to silicon IGBTs and MOSFETs [7] [6].

When reliability is essential, fault tolerance is increased with the use of redundant systems [8]. In the electrical drive context, multiphase (more than three phases) machines are considered one of the most promising technologies for fault tolerance [8], [5].

Multiphase inverters can be considered redundant by definition because when one of the phases is open, another phase can compensate for the power loss. However, when all phases are connected to a single neutral, with a variety of phases under failure, the system can cause complete inverter failure [8]. To minimize this problem, in [9] a complete bridge topology for each phase is presented. This makes the coils and the control galvanically isolated. Nonetheless, this topology presents lower efficiency and higher cost.

Still, in the context of redundancy and fault tolerance, an alternative is the use of multi-star electrical machines because they can also operate with open phases generated by faults. Considering the control aspects, when comparing the multiphase to the multi-star topologies, the latter requires less processing resources [8] and allows implementation of consolidated control methods based, e.g., on three-phase systems [9]. Some works present multi-star drive topologies for permanent magnet synchronous machines, e.g., with 3 and

"Manuscript received 08/31/2021; first revision 12/07/2021; accepted for publication 05/02/2022, by recommendation of Editor Marcelo Lobo Heldwein. <http://dx.doi.org/10.18618/REP.2022.2.0033>"

4 three-phase stars in [10] and [8], respectively. On the hand, it is also possible to use multiphase multi-star machines, i.e., machines with more than three phases and more than one star. Reference [11] presents a multi-star (three stars) five-phase asymmetrical electrical machine; however, with no experimental results. Based on the previous contextualization, the main contributions of this paper are listed below.

1. The design and experimental testing of a VSI SiC MOSFET multiphase inverter with independent drive and control capability of up to 15 phases. Therefore, the designed inverter can be used as a platform for driving and testing a wide range of multiphase and multi-star electrical machines. It allows driving machines with up to fifteen phases, making it a powerful drive and control experimental bench for multiphase electrical machines.
2. The control and modulation of an inverter implemented with a certified microcontroller for the automotive line using the GTM (Generic Timer Module) to activate the 30 independent static power switches.
3. A drive and testing of YASA-type electrical with five different electrical connections. The machine is driven in a standard three-phase system, in multiphase connections with 5 and 15 phases, in a multi-star connection with 5 independent three-phase stars, and in a multiphase multi-star connection with 3 independent five-phase connection.

This work is organized as follows: In Section II the topology of the inverter and its design characteristics are described. Then, in Section III the machine models are addressed. After, in Section IV the experimental results are presented and discussed. Section V presents the main conclusions.

II. VSI INVERTER DESIGN

This section presents the description of the designed inverter in terms of its hardware and software.

A. Hardware

The general structure of the VSI inverter power circuit proposed in this work is shown in Figure 1. In this circuit there are 30 power switches, each switch being commanded by a signal identified as S_n , where the subscript n identifies the switch number. Each pair of switches, connected between the V_{dc} terminals, forms an inverter arm. The midpoint between the switches is connected to the terminal of the machine.

It is important to highlight that it is possible to drive the 15 inverter arms independently. So, to use all inverter arms the designed inverter can drive a multiphase machine limited to 15 phases and can drive a five-star three-phase system or three-star five-phase system. Other connections are also possible if fewer inverter arms are used such as seven, nine, eleven, or thirteen multiphase machines or a two-star seven-phase machine.

It should be noted that in symmetrical multi-star topologies, the electrical systems can be isolated and operate with a phase shift between stars by an angle β that can be defined by $\beta = 360/(n_{star}m)$ where n_{star} is the number of stars in the

circuit and m is the number of phases.

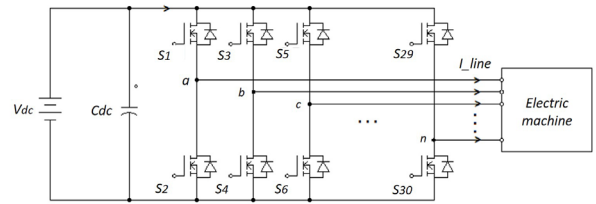


Fig. 1. Power circuit topology of the designed inverter.

The Figure 2 shows the main subsystems and the simplified structure of the inverter operation. To detail the developed project, the circuits were divided into LV (low voltage) and HV (high voltage). The power circuits (HV) are galvanically isolated from the control circuit (LV) at all interfaces. In Figure 2 it is possible to see the representation of the circuits that have galvanic isolation. The designed rated V_{dc} bus voltage is 850 V and the effective current in each arm is 35 A.

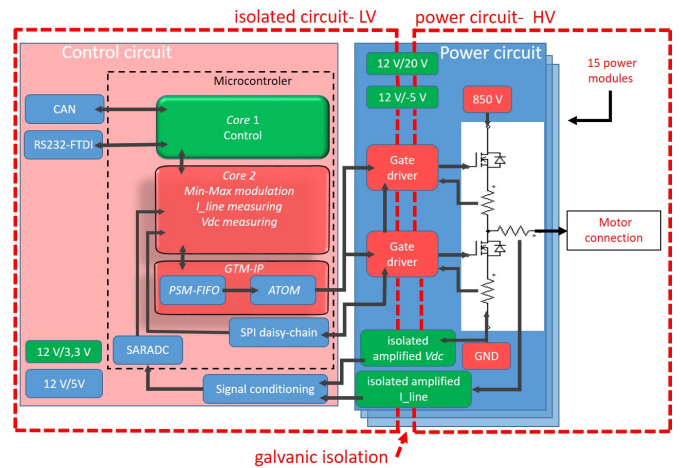


Fig. 2. Electronic topology of the multiphase inverter.

Each static switch is driven, detected, and autonomously controlled by independent gate driver circuits, configured with SPI (Serial Peripheral Interface) communication interface. The gate driver model STGAP1AS from STMicroelectronics was used, because it is certified for automotive application, is appropriate for the SiC MOSFET used (model SCTWA50N120 from STMicroelectronics), allows controlling of the dead time in activation between switches of the same power arm without dependence on the microcontroller, and has galvanic isolation.

Due to the high number of boards, cables with different lengths between the power arms are required, thus introducing different delays and noise in the drive. To minimize these interferences, an interlocking characteristic of the gate drivers was used, defining a digital filter in the input signals of 70 ns and a delay time between the activation of the power switches of the same power arm.

SPI communication is used for setting the basic control parameters. Modulation of the power switches is performed independently and directly between the control side of the gate drive and the microcontroller (model SPC58EE84E7QMSAR

from STMicroelectronics). The signals are generated through the PWM Min-Max Injection modulation [12] and sent to the GTM module (Generic Timer Module) intrinsic to the microcontroller. This module uses a ring operating buffer, with the duty cycle data for each modulator cycle, previously updated. The control and power system can operate with a switching frequency of up to 100 kHz, that is, with a frequency up to 10 times higher than the frequencies used in traditional inverters that use silicon IGBTs.

The phase currents are monitored by a 1 mΩ shunt resistor. The signal is then conditioned by a precision amplifier with rail-to-rail capacitive isolation and voltage gain of 8.2. The differential signal from the 15 outputs is then sent to the control board which has a signal conditioner. To read the 15 currents and ensure the correct phase shift, a SARADC (Successive Approximation Analog to Digital Converter) signal converter was used.

The voltage of the V_{dc} bus is also monitored by one of the power boards to minimize possible oscillations in the machine phase voltage by applying a correction to the modulation index of the system. Figure 3 shows a photograph of the designed inverter.

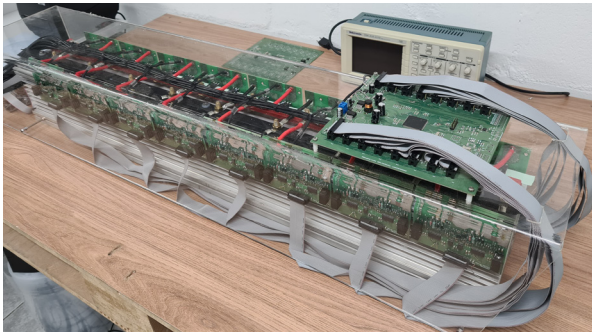


Fig. 3. Photograph of the prototype.

B. Software

The software was developed in C programming language using a tool of the SPC5 Studio[®] package. The structure of the software was subdivided into four main submodules: boot module, core 1, core 2, and GTM module.

The main boot module is responsible for defining the initial parameters such as the microcontroller's operating parameters, setting limits for the operation of power modules, machine data, connection type, number of phases, and number of stars, among others.

In core 1 the control of the machine is carried out. For the initial tests performed and presented in this paper, scalar control was implemented.

Core 2 is responsible for reading the peripherals and producing the modulating signals for each of the phases. It has a cyclic period of 50 μ s, i.e., 20 times the maximum fundamental modulating frequency specified for the project. The amplitude modulation index m_a is given by Equation (1), where the peak value of the fundamental component of phase voltage $V_{Phase_{max}}$ is corrected by the V/F curve factor.

$$m_a = \frac{V_{Phase_{max}}}{V_{dc}/2}. \quad (1)$$

The operation loop of core 2 is responsible for calculating the modulation vector used to drive the static switches.

The key time connected in the sine modulation is given by the interval between the intersections of the modulation and the carrier signal (sawtooth waveform) in which the modulation voltage is higher than that of the carrier. The intersections of these two signals can be found accurately if the modulation is continuously monitored, which is equivalent to being sampled infinitely. This is only possible in analog implementation. Currently, most implementations are based on digital processors and it is impossible to have infinite sampling and even a large sampling of reference signals, given the fact that the same processor is used for other control tasks.

The project considers the carrier frequency f_p fixed at 20 kHz for the fundamental frequency of modulation signal f_m in the range of 10 to 200 Hz; that is, e.g., for a modulating frequency of 10 Hz, the ratio between the carrier and the modulation frequencies, given by the modulation frequency index (m_f), Equation (2), is 2000. For 200 Hz the ratio is 100 times, still ensuring stability in the discretized system [13].

$$m_f = \frac{f_p}{f_m}. \quad (2)$$

However, for fundamental modulation frequency in the range of 201 to 1000 Hz, the frequency modulation index is set to 100 times to ensure stability in the [13] system. Thus, the carrier frequency becomes variable according to the frequency of the modulator. As an example, if the desired modulation frequency is 250 Hz or 1000 Hz the carrier frequency will be 25 kHz and 100 kHz, respectively. A complete phase voltage cycle is discretized according to Equation (3) for each of the phases and stars. The number of samples is identical to the frequency modulation index m_f .

$$V_{phase}[n_x][m_x][x] = m_a \sin(x\theta_{res} + m_x\theta_{phase} + n_x\theta_{star}) \quad (3)$$

where, θ_{phase} is the angle of lag between phases, m_x ranges from $\{0, 1, \dots, (m-1)\}$, $n_x = \{0, \dots, (n_{stars}-1)\}$, and $x = \{0, 1, \dots, (m_f-1)\}$. The modulation resolution angle (θ_{res}), in degrees, is given by Equation (4).

$$\theta_{res} = \frac{360}{m_f}. \quad (4)$$

The Min-Max Injection modulation method was implemented. Thus, using the phase voltage of Equation (3), the minimum and maximum vectors for all phases of the discretized signal can be determined by Eqs. (5) and (6), respectively.

$$MIN[n_x][x] = \min_{fn \in \{1, 2, \dots, m\}} V_{Phase}[fn][x] \quad (5)$$

$$MAX[n_x][x] = \max_{fn \in \{1, 2, \dots, m\}} V_{Phase}[fn][x]. \quad (6)$$

The common mode voltage vector v_{cm} for Min-Max Injection Modulation is given by Equation (7).

$$v_{cm}[n_x][m_x][x] = \frac{MAX[n_x][x] + MIN[n_x][x]}{2}. \quad (7)$$

The time vector DT , proportional to the carrier signal period T , for each of the phases and stars for the Min-Max

Injection Modulation method is then obtained by Equation (8).

$$DT[n_x][m_x][x] = \left((V_{Phase}[n_x][m_x][x]) - (v_{cm}[n_x][m_x][x]) \right) T. \quad (8)$$

III. ELECTRICAL MACHINE MODEL AND DESCRIPTION

The designed inverter is tested driving five different electrical connections on a YASA machine prototype, which is a surface permanent magnet synchronous rotary electric machine with axial flux in the air gap, with double rotor and segmented armature (YASA - Yokeless and Segmented Armature). The simplified geometrical model, containing the electromagnetic components of the machine, is shown in Figure 4.

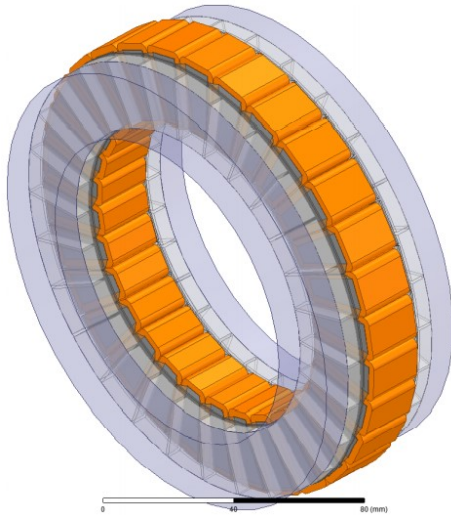


Fig. 4. Geometrical model of the YASA machine prototype [14].

This topology has a yokeless armature, which allows the use of grain-oriented laminated electrical steel, resulting in an increased power density and efficiency [14]. Goltz [14] developed a symmetric multiphase YASA machine with $Q_a=30$ armature segments using grain-oriented laminated electrical steel, slots with double-layer concentrated windings (tooth-coil), and $2p=32$ poles.

The machine can operate with 3, 5, or 15 phases by properly connecting the windings. This is possible by manually reconnecting the coils of the machine, since each coil terminal is accessible, as shown in the photograph of the prototype in Figure 5. In order to operate with the desired number of phases, the connections between coils must follow the phasor diagrams presented in Section IV of this paper for each specific case. Additionally, the inverter must be configured to the corresponding electrical connection.

In addition to the 3, 5, or 15-phase configurations, it is possible to operate with symmetrical multi-star connections with 3 and 5-phases by properly grouping isolated neutrals. All electrical systems are balanced in star connections without the need for a neutral.

This machine has double rotational symmetry, obtained by two base machines, i.e., $Q_a/2p = 15/16$. Therefore, only a

half machine, as shown in Figure 6, can be used to represent the induced voltage phasors, since the other half machine has exactly the same voltage phasors. The connection between the two base machines can be in series or parallel. In this case study, series connections were used.

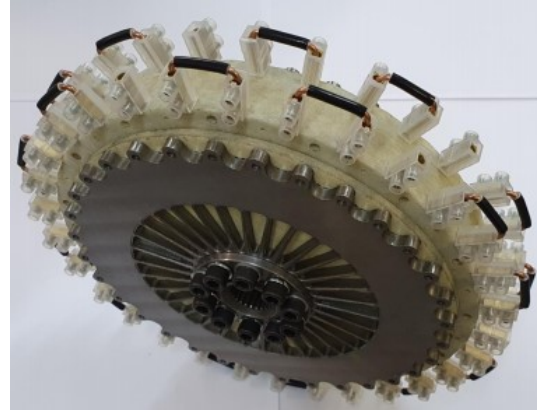


Fig. 5. Photograph of the YASA machine prototype [14].

The smallest electrical phase shift $\Delta_{e1C_y C_{y\pm 1}}$ between adjacent windings for the fundamental component of induced voltage can be defined by Equation (9) [14], where the subscript y , in the interval $[1, Q_a]$, identifies the armature segments identified in Figure 6. The first segment was named here as C_1 and positioned in the center of the armature of the base machine. However, such numbering could be moved to any other initial position. Based on Equation (9), it can be deduced that for a base machine with $Q_a=15$ armature segments and $2p=16$ poles, the smallest electrical angle between, e.g., C_1 and C_2 is $\pi/15$, i.e., 12 electrical degrees.

$$\Delta_{e1C_y C_{y\pm 1}} = \pi \frac{Q_a - 2p}{Q_a}. \quad (9)$$

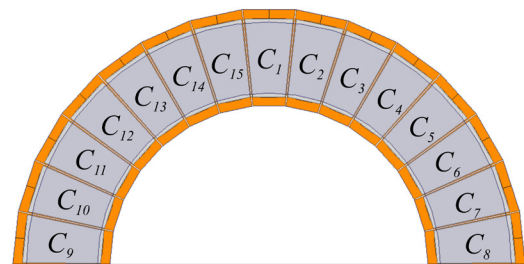


Fig. 6. Nomenclature and arrangement of coils in the base machine.

For the construction of the star of slots of the open-circuit induced voltage of the fundamental component of induced voltage in the base machine it is necessary to determine the electrical angular phase shift between a reference coil and any other coil in the base machine.

Considering that the coils are wound in the same direction, the electrical angular phase shift between the C_1 reference coil and any other coil C_y can be calculated by Equation (10) [14]. For example, using Equation (10) it is possible to obtain the phase shift between the fundamental components of induced voltage between coils C_1 and C_3 , i. e., $\delta_{e1C_1 C_3}$, which is 24 electrical degrees.

$$\delta_{e1C_1C_y} = \pi \left(\sin\left(\frac{\pi}{2}(y-1)\right) - (y-1) \frac{Q_a - 2p}{Q_a} \right). \quad (10)$$

It should be noted that y can vary from 1 to Q_a/t_p , where t_p is the number of base machines (two for the current prototype). Considering the base machine, the phasor diagrams of the balanced polyphase electrical systems using all coils for $m = 15, 5$ and 3 , can be drawn, as shown in Figures 12, 10 and 8, respectively.

In Figures 12, 10 and 8 it is possible to observe that the 15-phase machine has a unitary distribution factor, whereas for 5 and 3-phase connections it is given by the vectorial sum of the phasors that compose a phase. Therefore, the distribution factor is lower than one for 5 and 3-phase connections.

Additionally to the previously mentioned connections, it is possible to drive the machine with two multi-star topologies. The first, shown in Figure 14 has 5 isolated stars of 3-phase electrical systems. The second, shown in Figure 15 has 3 isolated stars of 5-phase electrical systems. It can be observed that in the multi-star connection the distribution factor is unitary. In this way, the multi-star systems have the same electromechanical conversion performance for the fundamental component as the 15-phase machine. However, the multi-star connections can significantly reduce the complexity of the control and the need for high-performance processing resources.

Even though the machine can be driven with several different electrical connections, the electrical equations that describe the model of a permanent magnet synchronous machine in the synchronous domain referenced to the rotor are described in Equation (11) and (12).

$$v_d = R i_d + L_d \frac{di_d}{dt} - p \omega_m L_q i_q \quad (11)$$

$$v_q = R i_q + L_q \frac{di_q}{dt} + p \omega_m (L_q i_q + \Psi_{pm}) \quad (12)$$

where, v_d, v_q , are the voltages in the synchronous reference (d-q), Ψ_{pm} the fundamental magnetic flux produced by the permanent magnets, L_q, L_d are the synchronous inductances, R the stator resistance, i_d, i_q the synchronous stator currents, ω_m the angular electric speed, and p the number of pole pairs. The torque equation for the fundamental current for any of the electrical connections can be obtained with Equation (13).

$$T_e = n_{star} \frac{m}{2} i_q p (i_d (L_d - L_q) + \Psi_{pm}) \quad (13)$$

where n_{star} is the number of stars. Equation (13) is a standard equation for torque calculation in synchronous machines, except for the term “ n_{star} ”, which is proposed in this paper. The assumption considers that the torque can be computed by the multiplication of the torque that would be obtained by a single star of the multi-star system multiplied by the number of independent stars n_{star} . Although this is an approximation, it is possible in this topology since there is little interaction between the magnetic flux of other stars once the mutual inductance between windings of the isolated stars in this topology with segmented armature is very low.

It is well-known that the 3-phase electrical system can be converted to a synchronous reference system using the Clarke-Park transformation given by Equation (14). This transformation is valid for the fundamental component of electric and magnetic quantities.

$$\begin{bmatrix} S_d \\ S_q \\ S_0 \end{bmatrix} = \frac{2}{3} \begin{bmatrix} \sin \theta_r & \sin(\theta_r - \frac{2\pi}{3}) & \sin(\theta_r + \frac{2\pi}{3}) \\ \cos \theta_r & \cos(\theta_r - \frac{2\pi}{3}) & \cos(\theta_r + \frac{2\pi}{3}) \\ \frac{1}{2} & \frac{1}{2} & \frac{1}{2} \end{bmatrix} \begin{bmatrix} S_a \\ S_b \\ S_c \end{bmatrix} \quad (14)$$

where, S can be replaced by voltages, currents or magnetic fluxes, and θ_r is the electric angular position of the rotor.

Following the same principle, in machines with a high number of phases (usually odd) the transformation matrix can be defined by Equation (15), where n is the n -th order harmonic of the variable being transformed and $\alpha = 2\pi/m$. Equation (15) is a transformation of a multi-phase system into synchronous references (dq) of fundamental and n -th harmonic order components.

It is worth mentioning that multiphase machines often make use of current harmonic injection to increase torque and power density. For this reason, Equation (15) is presented in a generalized form, including a n -th harmonic order. It is noteworthy that for the multi-star connection, the synchronous reference magnitudes are valid for each of the stars individually. This approach is possible because the mutual inductances between the phase coils of this topology are low, so there is no significant coupling between the different stars.

IV. EXPERIMENTAL RESULTS

To validate the inverter design, a prototype was developed as can be seen in Figure 5. The experimental tests were carried out on a bench shown in Figure 7, driving the motor described in Section III.

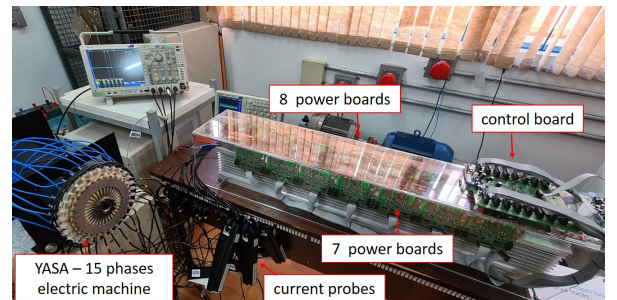


Fig. 7. Test bench: 15-phase inverter prototype (right) and YASA machine (left).

During the tests, the machine was driven with 25 Hz/ 93.5 rpm and with effective phase-current of approximately 3 A, for the purpose of comparison between the different electrical connections. The tests were carried out to validate the flexibility for driving machines with different electrical connections. The basic parameters of the prototype of the electrical are described in Table I.

$$\begin{bmatrix} S_d \\ S_q \\ S_{d3} \\ S_{q3} \\ \vdots \\ S_{dn} \\ S_{qn} \\ S_0 \end{bmatrix} = \frac{2}{m} \begin{bmatrix} \sin \theta_r & \sin(\theta_r - \alpha) & \sin(\theta_r - 2\alpha) & \dots & \sin(\theta_r + 2\alpha) & \sin(\theta_r + \alpha) \\ \cos \theta_r & \cos(\theta_r - \alpha) & \cos(\theta_r - 2\alpha) & \dots & \cos(\theta_r + 2\alpha) & \cos(\theta_r + \alpha) \\ \sin 3\theta_r & \sin 3(\theta_r - \alpha) & \sin 3(\theta_r - 2\alpha) & \dots & \sin 3(\theta_r + 2\alpha) & \sin 3(\theta_r + \alpha) \\ \cos 3\theta_r & \cos 3(\theta_r - \alpha) & \cos 3(\theta_r - 2\alpha) & \dots & \cos 3(\theta_r + 2\alpha) & \cos 3(\theta_r + \alpha) \\ \vdots & \vdots & \vdots & \vdots & \vdots & \vdots \\ \sin n\theta_r & \sin n(\theta_r - \alpha) & \sin n(\theta_r - 2\alpha) & \dots & \sin n(\theta_r + 2\alpha) & \sin n(\theta_r + \alpha) \\ \cos n\theta_r & \cos n(\theta_r - \alpha) & \cos n(\theta_r - 2\alpha) & \dots & \cos n(\theta_r + 2\alpha) & \cos n(\theta_r + \alpha) \\ \frac{1}{2} & \frac{1}{2} & \frac{1}{2} & \dots & \frac{1}{2} & \frac{1}{2} \end{bmatrix} \begin{bmatrix} S_1 \\ S_2 \\ S_3 \\ S_4 \\ \vdots \\ S_m \end{bmatrix} \quad (15)$$

TABLE I
YASA MOTOR PARAMETERS OF THE BASE MACHINE

Parameters	3 ϕ	5 ϕ	15 ϕ	5star-3 ϕ	3star-5 ϕ
R_s (Ω)	0.83	0.50	0.17	0.17	0.17
L_{d1} (mH)	10.13	6.12	2.09	2.09	2.09
L_{q1} (mH)	10.13	6.12	2.09	2.09	2.09
Ψ_{pm} (mWb)	81.7	65.1	38.0	38.0	38.0

A. Experimental Results with the Multiphase YASA Machine

This Section describes the tests with the multiphase YASA machine operating with five distinct electrical connections.

1) *Three-Phase Connection*: Considering the base machine, the phasor diagrams of the balanced polyphase electrical systems using all coils for $m=3$, can be drawn, as shown in Figure 8.

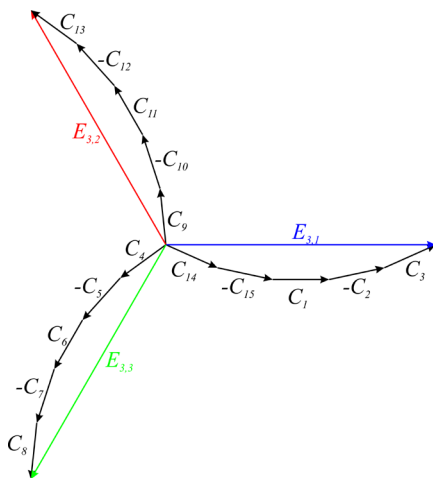


Fig. 8. 3-phase connection diagram.

where, C_y is the voltage phasor of a given coil shown in Figure 6 and $E_{m,ph}$ is the amplitude of the phase voltage phasor. The subscript m represents the total number of phases and ph the number of a certain phase of this system. The DC bus voltage used in this test was 140 V, with a modulation index of 0.58, which represents an imposed phase peak voltage equal to 40.6 V. Figure 9 shows the result of the electrical currents obtained experimentally with the inverter by feeding the machine with the three-phase connection.

In this case, only three inverter arms of the power module were used. Through FFT analysis it is possible to observe that the maximum amplitude variation between the phases of the fundamental component was 0.05 A. It is important to highlight that this small imbalance is not necessarily

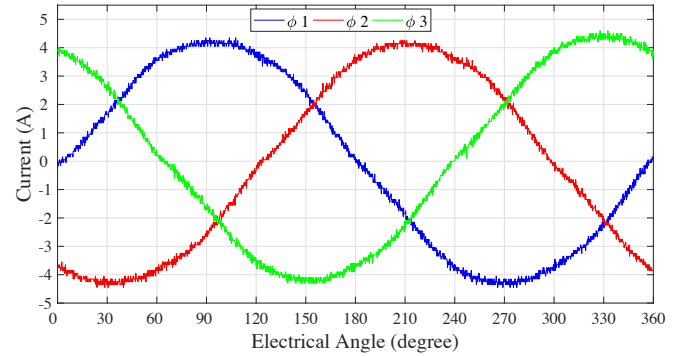


Fig. 9. Phase currents waveforms of 3-phase winding connection.

generated by the inverter, but may also be due to a small imbalance in the induced voltage or even due to the difference between parameters of the equivalent circuit of the phases. Additionally, as expected, the phase shift between the three phases is 120 degrees. Therefore, it can be characterized as a balanced system.

2) *Five-Phase Connection*: Based on the machine model, and Equation (9) and (10), it was possible to construct the phasor diagram of the fundamental component of the machine with the five-phase connection, as shown in Figure 10. The angular shift between adjacent fundamental voltage phasors in the 5-phase system is 72 degrees. To perform this test, 140 V was used on the DC bus with a modulation index of 0.494.

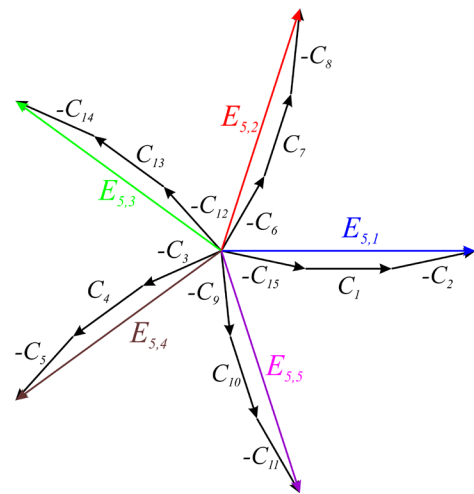


Fig. 10. 5-phase connection diagram.

Figure 11 shows the results of electric current in each of the 5 phases of the system. Through the FFT analysis, it was observed that the maximum variation between the amplitude

of currents of two phases was 0.14 A. As discussed for the three-phase system, the small imbalance in amplitudes cannot be attributed to the inverter, although the investigation of the cause of the imbalance has not been further investigated. The angle between the currents of the adjacent phases is 72 degrees, as expected.

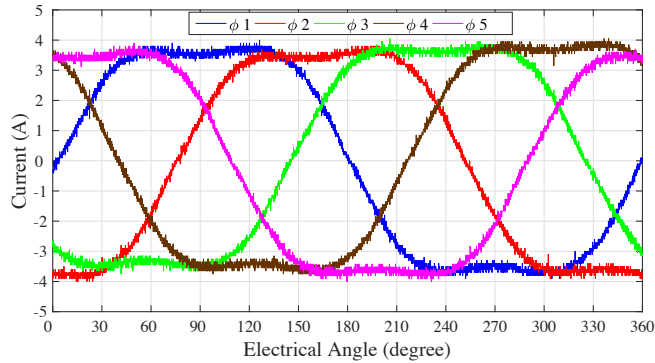


Fig. 11. Phase currents waveforms of 5-phase winding connection.

3) *Fifteen-Phase Connection*: Based on Equation (9) and (10), it was possible to construct the phasor diagram of the machine to operate with 15 phases, as shown in Figure 12. In the 15-phase topology, the distribution factor is unitary, because only one induced voltage coil from each base machine is connected per phase. This features a phase impedance of the machine with 1/5 of the three-phase system and consequently occurs a reduction of the induced voltage. These characteristics make it possible to reduce the voltage level of the DC bus and the modulation index for the same effective load current of the three-phase and 5-phase connection topologies. The voltage used on the DC bus was 34 V and the modulation index was 0.419.

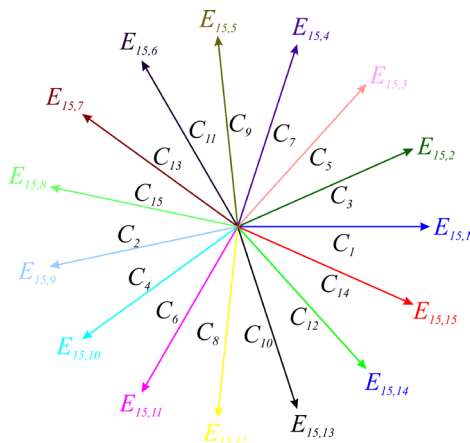


Fig. 12. 15-phase connection diagram.

The current curves obtained for the 15-phase machine are shown in Figure 13. Through the FFT analysis of the current signals, a low imbalance in the amplitude of the currents was observed with maximum amplitude variation between two phases of 0.20 A. The angular shift between the adjacent phases, observed is 24 degrees, as expected.

It can be observed in Figure 13 that current waves presented distortion close to the zero cross. This distortion comes from the ratio between the active switch time and the delay time

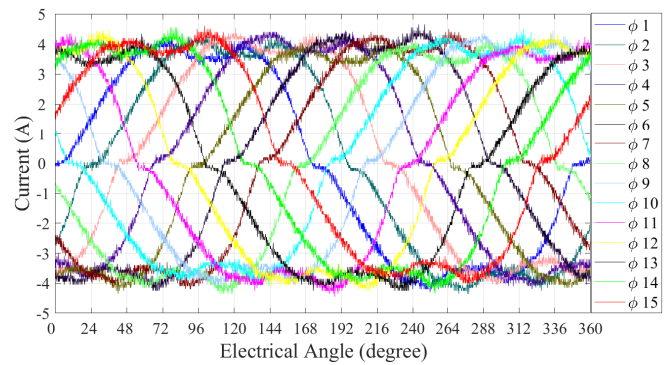


Fig. 13. Phase currents waveforms of 15-phase winding connection.

D_t on the gate driver (dead-time). The D_t time is injected by the gate driver to avoid simultaneous activation between the switches of the same power arm. This causes the T_{on} time to suffer this attenuation caused by the time D_t which generates the distortion visualized in the current around zero-crossing. Different compensation techniques are discussed in the literature, including the study of geometric modulation techniques and direct compensation models where through the analysis of the harmonic component of the load current a compensation time is added to the active time of the switch near zero-crossing [15].

4) *Multi-star Winding Connection*: In addition to the connections previously addressed, the machine can be driven with two multi-star topologies using all 15 coils of the base machine. The first topology has five isolated stars. Each star is composed of a three-phase electrical system as shown in Figure 14, where $E_{m,ph}^{n_{star}}$ represents the phase voltage phasor with its subscript designating the number of phases m , a particular phase ph and the superscript n_{star} represents the number of a certain star. The second multi-star topology, shown in Figure 15, has three isolated stars composed of 5-phase electrical systems.

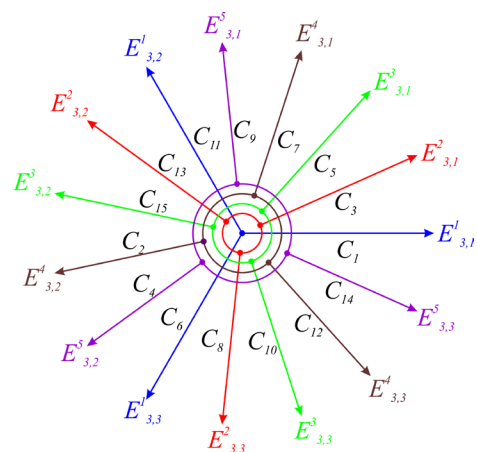


Fig. 14. 5-star 3-phase connection diagram.

It is possible to observe in Figures 16 and 17 that the currents of the phases of the three-phase and 5-phase subsystems, in a star, are shift by 120 degrees and 72 degrees, respectively. The shift between the same phases of different stars, such as $ph = 1$, is 24 degrees for adjacent stars. Through the FFT analysis of the currents of Figure 16, a low

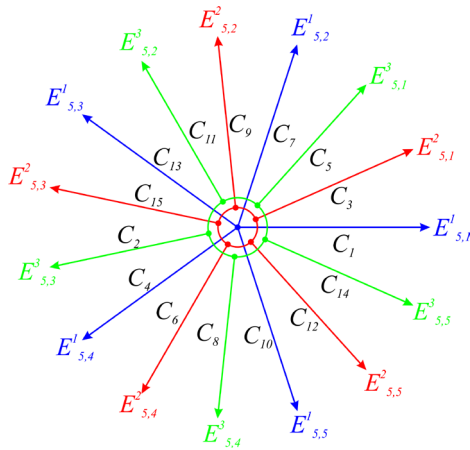


Fig. 15. 3-star 5-phase connection diagram.

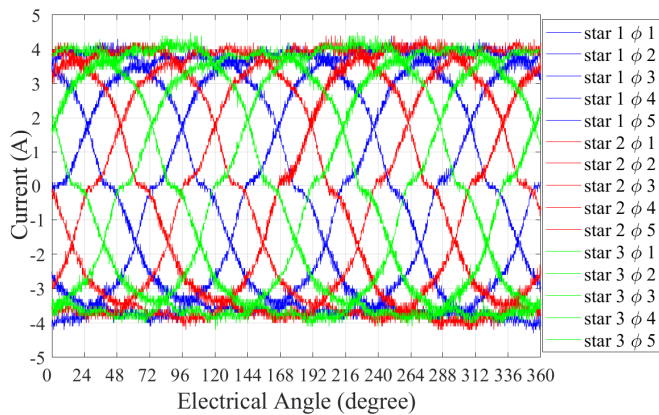


Fig. 17. Phase currents waveforms of 3-star and 5-phase winding connection.

imbalance in the amplitude of the currents was observed with maximum variation between two phases of 0.020 A and 0.19 A, respectively.

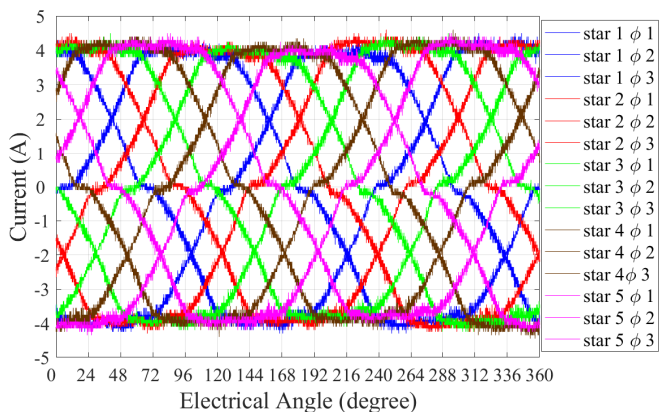


Fig. 16. Phase currents waveforms of 5-star and 3-phase winding connection.

In the same way, as in the system with 15 phases, the current waves also presented distortion close to zero-crossing. The reason that generated the distortion in the system with 15 phases can be extended to the multi-star model since the operating parameters and voltage levels are the same as those applied to the system with 15 phases.

In this way, the characteristics previously mentioned give the multi-star connections the same performance of electromechanical conversion for the fundamental component as the one obtained in the 15-phase machine. However, the multi-star connection can significantly reduce control complexity and the need for high-performance processing capabilities.

5) *Harmonic Analysis*: The low order harmonic composition of the electrical currents obtained by FFT is shown in Figure 18. As expected, all electrical connections do not present zero sequence currents. For example, the 3-phase systems do not contain third-harmonic and multiples. The equivalent is valid for 5 and 15-phase systems.

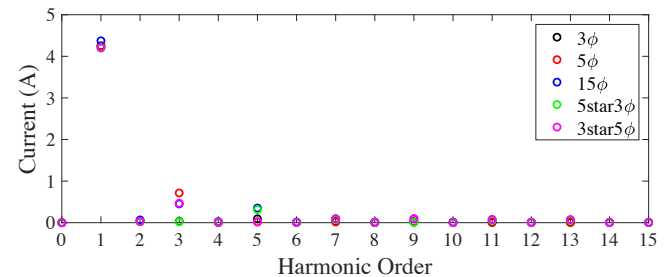


Fig. 18. The phase current spectrum of 3, 5, 15, 3-stars 5-phases and 5-stars 3-phase winding connection.

In the 5-phase system, the circulation of the third harmonic current was observed with 16.87 % of the fundamental. In the case of the system with 15 phases, two harmonics components became greater than zero: the third and fifth-order, representing 10.33 % and 8.04 % of the fundamental current, respectively. The presence of these harmonic components is generated mainly by the presence of these components in the induced voltage of the prototype of the YASA machine developed by [14]. Another factor that contributes to the increase in harmonic content is the presence of dead time used to avoid simultaneous activation of the power switches of the same arm.

B. Open-Phase Fault Operation

Redundancy and fault tolerance is one of the main advantages of multi-phase and/or multi-star systems. Thus, the functionality of the machine and inverter even in a fault condition is validated qualitatively. The tests were restricted to the 5-phase connection. The simulated failures consider the total opening of one of the phases of the system, evaluation of the currents in the other phases, and verification of the maintenance of the synchronism in the machine.

In the test, the phase identified as 5 at the time instant defined as (A) in Figure 19 was opened. The effective value of the fundamental component of current in phase 5 has become zero. The maximum imbalance between that observed after opening one of the phases was 1.05 A. Then, at the instant of time (B) identified in Figure 19, phase 3 of the five-phase machine was also open.

The effective value of the fundamental component of the current in phases 3 and 5 that were open was zero, while the maximum current imbalance between the active phases was 0.94 A. It was observed that under fault operation conditions without any control technique applied there is a significant

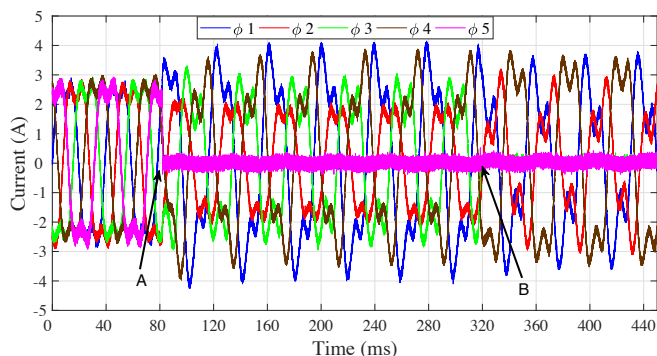


Fig. 19. The Currents in the machine with 5 phase connection without failure in the interval [0, A], with a fault caused by opening in phase 5 at interval [A, B] and with a fault caused by openings in phases 5 and 3 in the interval [B, 450 ms].

imbalance between currents. However, the machine continued to operate and maintained synchronization.

C. Operation with High Modulating and Switching Frequencies

The validation of the inverter functionality in terms of the fundamental frequency and carrier frequency was performed by feeding a load with and resistor and inductor (RL) connected in series. For this, the modulating frequency of 1 kHz and the carrier frequency of 100 kHz was applied to the load. The tests were performed on a bench with an RL load. The inductors have been developed to present approximately the same inductance as the 15-phase machine, i.e. $2.09 \times 2 \approx 4.3$ mH. This inductance is considered for the connection of two groups of coils in series. The modulation index used for the tests was set at 0.4 and the voltage source bus $V_{dc} = 60$ V.

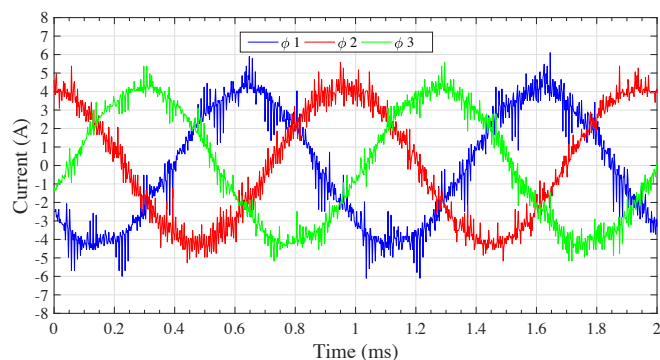


Fig. 20. Phase currents for 3-phase connection and modulation 1 kHz frequency.

The gate-to-source voltage of the power switches of an arm operating with a carrier frequency of 100 kHz is shown in Figure 21. It can be observed that the power switches have complementary signals. In addition, it is noted that the period of a cycle is $10 \mu\text{s}$, which proves the operation with the carrier frequency of 100 kHz.

In the test with RL load, a three-phase system was used, since the main objective is functionality in terms of switching frequency and fundamental operating frequency. The line current at the load for the three phases of the system is shown in Figure 20. It is possible to observe that the fundamental frequency, which is equal to the modulating frequency, in this

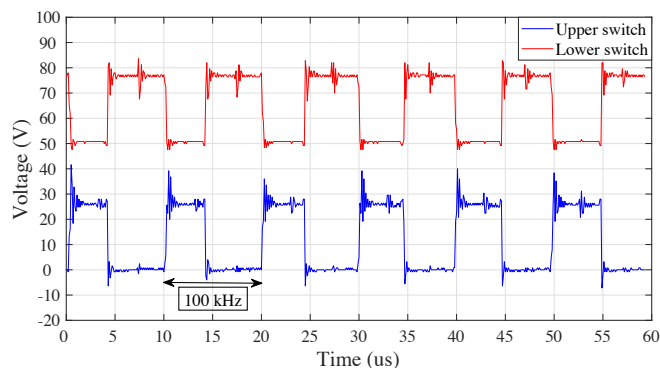


Fig. 21. Gate-to-source voltage of the power switches of an arm operating with carrier frequency of 100 kHz.

test is 1 kHz. From Figure 20 it is also possible to observe that the three currents have the same amplitudes and angular shift of 120 degrees between each other, which characterizes a balanced three-phase system, as expected.

V. CONCLUSIONS

In this work, the design of a VSI inverter with flexible drive capacity proved to be effective. It was found that, according to the literature, the use of high-performance multiphase and/or multi-star electrical machines combined with multiphase inverters can provide safety, redundancy, parallelism, and robustness to electrical traction systems. Thus, an inverter was designed to be used as a platform for testing machines with up to 15-phases. It was possible with the use of only one microcontroller to independently drive 30 static power switches. The functionality of the inverted was demonstrated with a test of five different multiphase and multi-star electrical connections on the same YASA machine. From the results presented it can be concluded that the multiphase inverter developed achieved the design objectives as it was used as a flexible platform for driving multiphase electrical machines with different connections and configurations and it operates with high fundamental and switching frequencies.

ACKNOWLEDGEMENTS

The authors thank STMicroelectronics® for donating components to the inverter. Additionally, this study was financed in part by the Coordenação de Aperfeiçoamento de Pessoal de Nível Superior - Brasil (CAPES) - Finance Code 001.

REFERENCES

- [1] IEA, *Global EV Outlook 2021*, IEA, Paris, 2021, disponível em: <https://www.iea.org/reports/global-ev-outlook-2021>. Accessed: May 2021.
- [2] M. Henke, G. Narjes, J. Hoffmann, C. Wohlers, S. Urbanek, C. Heister, J. Steinbrink, C. W. Rudiger, B. Ponick, "Challenges and opportunities of very light high-performance electric drives for aviation", *Energies*, vol. 11, no. 2, Feb. 2018, doi: 10.3390/en11020344.
- [3] R. S. Miranda, C. B. Jacobina, A. M. N. Lima, M. B. R. Correa, "Operação de um Sistema de

Acionamento com Motor de Seis Fases Tolerante a Falhas”, *Revista Brasileira de Eletrônica de Potência da SOBRAEP*, vol. 10, no. 1, pp. 15–22, Jun. 2005, doi:10.18618/REP.2005.1.015022.

- [4] D. Dujic, G. Grandi, M. Jones, E. Levi, “A Space Vector PWM Scheme for Multifrequency Output Voltage Generation With Multiphase Voltage-Source Inverters”, *IEEE Transactions on Industrial Electronics*, vol. 55, no. 5, pp. 1943–1955, Apr. 2008, doi:10.1109/TIE.2008.918468.
- [5] F. Scuiller, J.-F. Charpentier, E. Semail, “Multi-star multi-phase winding for a high power naval propulsion machine with low ripple torques and high fault tolerant ability”, in *IEEE Vehicle Power and Propulsion Conference*, pp. 1–5, Sep. 2010, doi: 10.1109/VPPC.2010.5729185.
- [6] I. López, E. Ibarra, A. Matallana, J. Andreu, I. Kortabarria, “Next generation electric drives for HEV/EV propulsion systems: Technology, trends and challenges”, *Renewable and Sustainable Energy Reviews*, vol. 114, pp. 109–336, Oct. 2019, doi: 10.1016/j.rser.2019.109336.
- [7] D. Tan, “Power Electronics: Historical Notes, Recent Advances and Contemporary Challenges”, *Eletrônica de Potência*, vol. 25, no. 4, pp. 386–394, Dec. 2020, doi:10.18618/rep.2020.4.00701.
- [8] G. Sala, M. Mengoni, G. Rizzoli, M. Degano, L. Zarri, A. Tani, “Impact of Star Connection Layouts on the Control of Multiphase Induction Motor Drives Under Open-Phase Fault”, *IEEE Transactions on Power Electronics*, vol. 36, no. 4, pp. 3717–3726, Apr. 2021, doi:10.1109/TPEL.2020.3024205.
- [9] J. W. Bennett, G. J. Atkinson, B. C. Mecrow, D. J. Atkinson, “Fault-Tolerant Design Considerations and Control Strategies for Aerospace Drives”, *IEEE Transactions on Industrial Electronics*, vol. 59, no. 5, pp. 2049–2058, May 2012, doi: 10.1109/TIE.2011.2159356.
- [10] S. Piepenbreier, J. Berlinecke, N. Burani, R. Bittner, S. Matichyn, F. Streit, M. Hofmann, R. Plikat, “Analysis of a Multiphase Multi-Star PMSM Drive System with SiC-Based Inverter for an automotive application”, in *PCIM Europe 2018; International Exhibition and Conference for Power Electronics, Intelligent Motion, Renewable Energy and Energy Management*, pp. 1–10, Jul. 2018.
- [11] Z. Kuang, B. Du, S. Han, K. Li, S. Cui, “Optimal Efficiency Control of Asymmetrical Fifteen Phase PMSM Based on Fuzzy Logic Control Theory”, in *IEEE Vehicle Power and Propulsion Conference (VPPC)*, pp. 1–6, Aug. 2018, doi: 10.1109/VPPC.2018.8604974.
- [12] B. M. Wilamowski, J. D. Irwin, *Power electronics and motor drives*, 2016, doi:10.1201/b11657-2.
- [13] H. A. A. Awan, T. Tuovinen, S. E. Saarakkala, M. Hinkkanen, “Discrete-Time Observer Design for Sensorless Synchronous Motor Drives”, *IEEE Transactions on Industry Applications*, vol. 52, no. 5, pp. 3968–3979, May 2016, doi: 10.1109/TIA.2016.2572105.
- [14] E. C. Goltz, *Estudo da Máquina Elétrica de Fluxo Axial com Duplo Rotor e Armadura Segmentada*, Tese (doutorado em engenharia), Programa de Pós-Graduação em Engenharia Elétrica, Universidade Federal do Rio Grande do Sul, Porto Alegre, Jan. 2021.
- [15] D.-H. Lee, J.-W. Ahn, “A Simple and Direct Dead-Time Effect Compensation Scheme in PWM-VSI”, *IEEE Transactions on Industry Applications*, vol. 50, no. 5, pp. 3017–3025, Sep. 2014, doi: 10.1109/TIA.2014.2303932.

BIOGRAPHIES

Rodrigo Parizotto was born in São Marcos, RS, Brazil, in 1987. He received the B.Eng. degree in Electrical Engineering from the University of Caxias do Sul (UCS) in 2015, and the M.Sc. degree in Electrical Engineering from the Federal University of Rio Grande do Sul (UFRGS), Porto Alegre, RS, Brazil, in 2021.

He is currently Project Manager in the company Inbrasel, working with the research and development of industrial machines. His research interests include the design and modeling of power inverters applied to electric mobility.

Evandro Claiton Goltz received the B.Eng. degree in electrical engineering from the Federal University of Santa Maria (UFSM), Santa Maria, RS, M.Eng. and Ph.D. degrees in electrical engineering from the Federal University of Rio Grande do Sul (UFRGS), Porto Alegre, RS, Brazil, in 2009, 2012 and 2021, respectively.

Currently he is working with NUPEDDEE/UFSM with the Laboratory of Electrical Machines. His research interests include design and modeling of electromagnetic devices and electric drives. Dr. Goltz is a member of the Brazilian Society of Electromagnetism.

Ederson dos Reis was born in Caxias do Sul, Brazil, RS in 1975. He received a degree in Electrical Engineering from the University of Caxias do Sul (UCS), Bento Gonçalves, RS, Brazil in 2015.

He is currently a managing partner of the company Style Equipamentos Eletrônicos. He has experience in the field of electrical engineering, with an emphasis on industrial electronics and electronic device development. He is currently studying at the Federal University of Rio Grande do Sul (UFRGS) with the aim of obtaining a master’s degree.

Paulo Roberto Eckert received the B.Eng., M.Sc. and Ph.D. degrees in electrical engineering from the Federal University of Rio Grande do Sul (UFRGS), Porto Alegre, RS, Brazil, in 2007, 2012, and 2016, respectively.

He is currently an Associate Professor with the Department of Electrical Engineering and a Researcher with the Laboratory of Electrical Machines, Drives and Energy, UFRGS. His research interests include design and modeling of electromagnetic devices and electric drives.